Ferrian high sanidine in a lamproite from Cancarix, Spain

KEES LINTHOUT AND WIM J. LUSTENHOUWER

Department of Petrology and Isotope Geology, Institute of Earth Sciences, Vrije Universiteit, De Boelelaan 1085, 1081 HV Amsterdam, The Netherlands

Abstract

Na-poor, Fe-bearing high sanidine from a lamproite near Cancarix (Spain) has $2V\alpha\|(010) = 37–43°$, and $C2/m$, $a = 8.598(15)$, $b = 13.050(26)$, $c = 7.209(17)$ Å, $\beta = 116.00(18)°$, $V = 727(2)$ Å^3. Rims of sanidine crystals against vugs contain up to 60 mole % $KFeSi_3O_8$ and up to 10 at.% Si and 6 at.% K above the stoichiometric requirement; otherwise, they have up to 4 mole % $\square Si_4O_8$ and 3 mole % $K_2O.Si_4O_8$ in solid solution. Their MgO content may reach 0.46 wt.%. The skeletons of mm sized blocky crystals (Baveno habit) indicate formation under moderate undercooling at temperatures not much above 725 °C. Feldspar formation was facilitated by a high diffusion rate due to low viscosity in a highly perpotassic melt, supersaturated by pressure release and diopside fractionation, upon extrusion of a huge volume of lava in a crater. After titanian potassium-richterite largely filled the interstices in the sanidine fabric, crystals of dalyite ($K_2ZrSi_6O_{15}$) and Fe-rich rims of sanidine and amphibole crystals were formed from an increasingly hydrous, silicic, ferric, and peralkaline residual melt. High rate nonequilibrium crystallisation caused the incorporation of excess SiO_2 and K_2O in the defect structure of the sanidine. Retrograde boiling initiated the escape of volatiles, causing the quenching, by which the disordered structural state and the nonstoichiometric composition of the sanidine were preserved.

KEYWORDS: ferrian sanidine, lamproite, dalyite, Cancarix, Spain.

Introduction

KFE-FELDSPAR can be synthesised in triclinic and monoclinic varieties (Hautefeuille and Perrey, 1888; Faust, 1936; Wones and Appleman, 1961, 1963) and extensive solid solution between $KAlSi_3O_8$ and $KFeSi_3O_8$ has been established experimentally as well (Lindqvist, 1966). In natural feldspars, however, iron is known at most as a minor element. Highest iron contents so far were reported from sanidine in lamproites, with a maximum of 4.95 wt.% Fe_2O_3 (Wagner and Velde, 1986).

In this paper we present petrographical and mineralogical data for iron-bearing sanidine from a Spanish lamproite. The rims of sanidine crystals, bordering vugs, contain up to 14.5 wt.% Fe_2O_3. As far as we know, this is the first report of natural feldspar with a composition dominated by the ferric component.

Setting and petrography

The sample is from the Late Miocene vent, standing out by erosion (much like the type-2 vent of Mitchell and Bergman, 1991) in the Cerro Negro, two km west of Cancarix in the province of Albacete, Spain. Field evidence indicates that the volcanic body, extending 1100 m NS and 800 m EW, was formed by a single extrusion, filling a crater with several tens of millions of m^3 of lava (Linthout *et al.*, 1988). The well developed flow-banding in the glassy margin of the body against the crater wall indicates the low viscosity of the lava.

Sanidine constitutes about 50 vol.% of the rock. It occurs in about four mm large subradiating skeletal aggregates of typically untwinned, 0.3 to 1 mm sized, euhedral, blocky, equant to elongate crystals (Fig. 1), thus displaying the Baveno habit (Woensdregt, 1982). Since there are no indications that sanidine formed by reaction between leucite and liquid, it appears to be a primary liquidus phase. Up to three mm large crystals of titanian potassium-richterite fill most of the interstices of the sanidine fabric. Ubiquitous miarolitic cavities, bordered by sanidine and amphibole, contain dalyite ($K_2ZrSi_6O_{15}$) as an accessory mineral (Fig. 2).

X-ray imaging shows that the sanidine is Fe-rich only in crystal rims bordering druses (Fig. 2),

Mineralogical Magazine, June 1993, Vol. 57, pp. 289–299

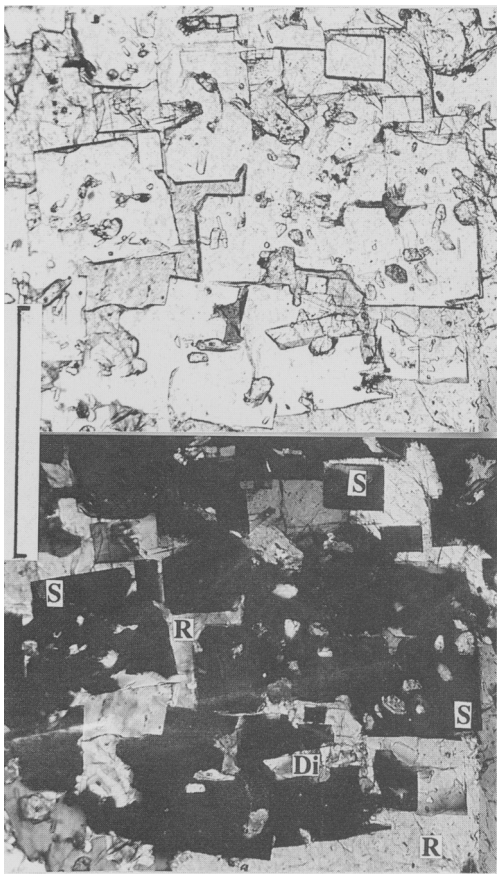

FIG. 1. Photomicrographs of cancalite, in plane polarised light and between crossed polars, showing the blocky skeletal habit of sanidine (S), interstitial titanian potassium-richterite (R), and diopside prisms (Di) forming euhedral inclusions in feldspar. Scale bar is 1 mm.

indicating that the Fe-rich sanidine formed at a very late stage, roughly coeval with the final crystallisation of amphibole and later than dalyite. Very fine needles of aegirine, crossing druses, have grown still later, conceivably from a vapour phase (cf. Lindsley *et al.*, 1971).

Early-formed minerals, mainly as inclusions in the sanidine crystals, are: olivine, as fresh, but corroded anhedral crystals and in peridotitic xenoliths; phlogopite, as corroded crystals with sagenitic exsolutions; diopside, in numerous euhedral prisms; apatite needles; and scarce crystals of ilmenite, occasionally intergrown with geikielite. Where not armoured by sanidine, diopside and phlogopite show replacement by titanian potassium-richterite, whereas olivine relics are corroded and mantled by enstatite. In its turn, orthopyroxene is mantled by and intergrown with the amphibole.

The volcanic rock, with titanian potassium-richterite as an important phase in the mode, should be grouped with the lamproites (Le Maitre, 1989). The norm of the sample features olivine (*ol*), acmite (*ac*), sodium metasilicate (*ns*) and potassium metasilicate (*ks*) but no leucite (*lc*) (Linthout *et al.*, 1988). Following Fuster *et al.* (1967), the presence in the norm of ol without lc characterises this lamproite as the type-variety cancalite. For a comprehensive review on lamproites, see Mitchell and Bergman (1991).

The compositions of the various minerals (Table 1) and the whole rock corroborate the cancalite of Cancarix data given by Nixon *et al.* (1984), Venturelli *et al.* (1984), Wagner and Velde (1986), and also those given by Best *et al.* (1968) on an American 'trachyte', which appears to be an orthopyroxene-free cancalite. However, as yet, dalyite and aegirine have not been described from lamproites elsewhere (Mitchell and Bergman, 1991) and the very high Fe^{3+} contents, as in the rims of sanidine crystals (Tables 2 and 3), have not been found in any rock.

Sanidine from Cancarix

Optical properties

The crystals are clear, transparent and show no alteration. The orientation of the optic axial plane is parallel to (010). The optic axial angle $2V_\alpha$ varies between 37 and 43° (measured in Na-light on a Zeiss universal stage) and displays a distinct dispersion $v > r$. These data are diagnostic of Na-poor high sanidine (Spencer, 1937; Su *et al.*, 1986). The structural state of alkali feldspars can be estimated from their composition and optic axial angle with a precision similar to that of models relying on lattice parameters; minor substitutions are claimed to have little effect (Su *et al.*, 1986). Thus neglecting Fe,Al substitution, $2V_\alpha \| (010) = 37–43°$ and $X_{Or + FeOr} = 0.95$ point to a structural state which in terms of the R^{3+} content of the T_1-site, can be expressed as $\Sigma t_1 = 0.58$ to 0.61.

Determination of 2V in the iron-rich rims was not possible, because of their small width. In accord with the optical properties of synthetic iron-sanidine (Wones and Appleman, 1961), the rims show a stronger birefringence and no change in optical orientation.

Cell dimensions

The X-ray powder-diffraction Guinier photograph shows sharp reflections, thus giving no clue

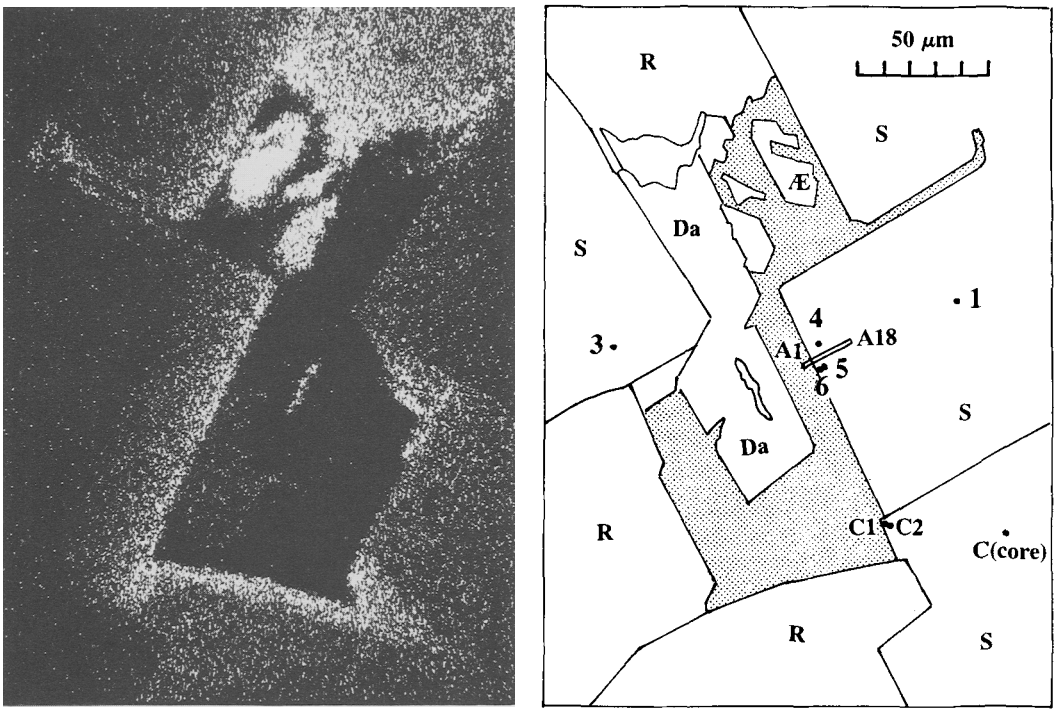

FIG. 2. Fe-$K\alpha$ X-ray image and drawing of cancalite of Cancarix showing crystals of sanidine (S), titanian potassium-richterite (R), dalyite (Da) and aegirine (Æ) around a miarolitic cavity. Contours of dalyite crystal drawn from a backscattered electron image. Note the Fe increase in feldspar and amphibole across the rims facing the vug. Sites of EMP analyses of Table 2 are indicated 1 to 6 (excl. #2, which falls outside the figure); the location of the SEM step scan (Fig. 3) is marked by the bar between A1 and A18; additional sites of SEM analyses C1, C2 and C(core), referred to in Table 3, are also indicated.

to the strong, but volumetrically insignificant, compositional changes across the rims of the crystals. Cell dimensions were computed from 21 reflections: *C2/m*; $a = 8.595(15)$; $b = 13.050(26)$; $c = 7.209(17)$ Å; $\beta = 116.00(18)°$; $V = 727(2)$ Å^3, which are similar to those given by Best *et al.* (1968) for a high sanidine with 3.83 wt.% Fe_2O_3 (Table 4; Fig. 4). According to Kroll and Ribbe (1987) the structural state of monoclinic alkali feldspars can be estimated from b and c^*; application of their formula $\Sigma t_1 = 72.245 - 3.1130b - 200.785c^*$, neglecting possible effects of Fe,Al substitution, leads to $\Sigma t_1 = 0.63$, which is of the same order as the values found via the optical and compositional data. The b–c plot illustrates the appreciable Fe content and the HT structural state of the sanidine of Cancarix (Fig. 4).

Chemical composition

Analytical methods. Electron-microprobe (EMP) analyses were performed with a Cambridge Instruments Microscan-9, with 15 kV acceleration voltage and 5×10^{-8} A specimen current on a Faraday cup. Well calibrated natural and synthetic stanards were used. The analyses were ZAF corrected with the Microscan-9 on-line correction program. To minimise mineral decomposition, sanidine was analysed with the electron beam in raster mode (2.5×3 μm^2). For the analysis of the rim the electron beam was placed at least 5 μm inside the grain boundary.

To study the compositional variation in the outer rims, scans with increments of 1 μm across these rims were made by quantitative scanning electron microscopy (SEM) using a JEOL JSM-6400, equipped with a Link eXL energy dispersive system. Standards used were orthoclase (K,Al,Si) almandine (Fe) and the same standards as used for EMP analysis for the other elements. The acceleration voltage was 15 kV, and to prevent the feldspar from decomposing during analysis, a specimen current of 5×10^{-10} A was applied, with the focussed beam in raster mode (1×1.25 μm^2).

Analytical results. A selection of six representa-

Table 1. Representative compositions and unit formulae of non-feldspar silicates from Cancarix.

	ol	en	di	aeg	amphibole		phlogopite		dalyite[a]
					core	rim	core	rim	
SiO_2	40.6	56.6	54.2	52.0	53.1	51.8	40.9	40.9	62.72
TiO_2		0.17	0.67	0.68	5.76	8.82	2.33	8.65	1.03
ZrO_2									19.39
Al_2O_3			0.32	0.07	0.56	0.20	12.1	8.78	0.08
Cr_2O_3	0.03	0.16	0.93						
Fe_2O_3		0.21*		26.7*					0.19[t]
FeO	10.4[t]	10.4*	3.61[t]	3.66*	4.82[t]	12.7[t]	3.39[t]	7.74[t]	
MnO	0.26	0.29	0.12	0.21	0.04	0.09		0.03	
NiO	0.32								
MgO	47.7	31.1	17.7	1.59	17.3	9.88	24.0	17.8	0.02
CaO	0.23	1.06	21.63	2.83	6.23	3.82			
BaO						0.23	0.18	0.37	0.32
Na_2O		0.09	0.27	11.3	4.35	5.55	0.17	0.41	0.14
K_2O				0.06	4.26	4.34	10.40	9.68	16.04
F					1.70	0.20	6.12	3.63	
O=F					-0.72	-0.08	-2.58	-1.53	
Total	99.54	100.08	99.42	99.1	97.40	97.55	97.01	96.46	99.93
calculation basis	4O	6O	6O	6O	23O	23O	22O	22O	15O
Si	1.00	1.99	1.99	2.01	7.67	7.68	5.92	6.00	6.00
Ti			0.02	0.02	0.63	0.98	0.25	0.95	0.07
Zr									0.91
Al			0.01		0.09	0.03	2.05	1.52	0.01
Cr			0.03						
Fe^{3+}		0.01		0.78					0.02
Fe^{2+}	0.22	0.31	0.11	0.12	0.58	1.58	0.41	0.95	
Mn	0.01	0.01		0.01		0.01			
Ni	0.01								
Mg	1.76	1.63	0.97	0.09	3.72	2.19	5.17	3.88	
Ca	0.01	0.04	0.85	0.12	0.96	0.61			
Ba						0.03	0.01	0.02	0.01
Na		0.01	0.02	0.85	1.22	1.60	0.05	0.12	0.03
K					0.79	0.82	1.92	1.81	1.96
F					0.78	0.09	2.80	1.68	

1: ol = olivine, di = diopside, aeg = aegirine; a: av. of six analyses, after Linthout et al. (1988); t: total iron as FeO or as Fe_2O_3; *: calculated from unit formula.

tive EMP analyses of spots in sanidine is listed in Table 2. The results of a SEM scan across the rim of a sanidine crystal are given in Fig. 3, and selected SEM analyses are listed in Table 3. The locations of most analysed spots in sanidine and of the SEM step scan are given in Fig. 2. The reliability of the feldspar analyses can be judged from the sum of the oxide weight percentages, which are all close to 100% for the EMP determinations; this applies also to the SEM results, except for the few obtained from sites within 3 μm of crystal boundaries. Moreover, the derived unit formulae based on eight oxygen atoms per formula unit (a.p.f.u.) easily meet the quality criteria based on comparison with the basic feldspar formula MT_4O_8.

The results confirm the K-rich (>16 wt.% K_2O), Na-poor (<0.45 wt.% Na_2O) and Fe-bearing composition of the larger inner parts of the crystals, as inferred from optical and X-ray powder-diffraction data. A strong decrease in Al content, from the cores to the rims, is accompanied by a simultaneous and consistent increase in Fe (Fig. 3). For a K-feldspar, the

Table 2. Selected EMP analyses[1] and unit formulae[2] of sanidine of Cancarix; feldspar end-members in mole % ; and consequent nonstoichiometry

	1	2	3	4	5	6
SiO_2	63.8	63.9	63.6	63.8	62.5	63.3
TiO_2			0.06		n.d.	n.d.
Al_2O_3	17.4	15.9	15.7	12.4	9.33	6.61
Fe_2O_3[t]	1.04	2.83	3.56	7.01	10.5	13.7
MgO	0.08	0.10	0.12	0.26	0.33	0.36
CaO	n.d.	n.d.	n.d.	n.d.	n.d.	n.d.
BaO	0.31	0.33	0.40	0.41	0.37	0.20
Na_2O	0.44	0.33	0.41	0.36	0.43	0.32
K_2O	16.1	16.3	16.1	15.8	15.6	15.3
Total	99.17	99.69	99.95	100.04	99.06	99.79
Si	2.994	3.007	2.993	3.030	3.043	3.081
Ti	-	-	0.002	-	-	-
Al	0.962	0.879	0.870	0.695	0.536	0.379
Fe^{3+}	0.027	0.100	0.126	0.250	0.383	0.500
Mg	0.006	0.007	0.008	0.018	0.024	0.026
Ba	0.006	0.006	0.007	0.008	0.007	0.004
Na	0.040	0.030	0.037	0.033	0.041	0.030
K	0.965	0.979	0.964	0.958	0.971	0.948
$(Na,K)Mg_{0.5}\ Si_{3.5}O_8$	1.2	1.4	1.6	3.6	4.8	5.2
$Ba\ Al_2\ Si_2O_8$	0.6	0.6	0.7	0.8	0.7	0.4
$Na\ Al\ Si_3O_8$	2.8	1.6	2.1	-	-	-
$K\ Al\ Si_3O_8$	92.2	85.1	83.5	67.9	52.2	37.1
$K\ Fe\ Si_3O_8$	3.0	10.0	11.8	25.0	38.3	50.0
Total	99.8*	98.7*	99.7*	97.3	96.0	92.7
nonstoichiometric surplus						
K (a.p.f.u.)	*	*	*	0.026	0.059	0.055
Si (a.p.f.u.)	*	*	*	0.111	0.146	0.278
equivalent $K_2O.Si_4O_8$ (mole %)	*	*	*	1.3	3.0	2.8
equivalent $\square Si_4O_8$ (mole %)	*	*	*	1.5	0.7	4.2

1: see Fig. 2 for locations (excl. #2); 2: based on eight oxygen; n.d.: none detected; t: total iron as Fe_2O_3; *: deviation from feldspar stoichiometry considered insignificant;

sample has a remarkable Mg content: by EMP and SEM, respectively, up to 0.36 and 0.46 wt.% MgO were found in the rims. These values are surpassed only by a 'Mg-rich' sanidine with 0.44–0.53 wt.% MgO (Smith and Franks, 1986).

The SEM analyses A6 and C1, within 3 μm from the crystal boundaries, gave the highest iron contents measured in the sanidine of this sample: 14.5 wt.% Fe_2O_3, with totals of 97.2 and 92.9 wt.%, respectively. These totals are low because the excitation volume of the electron microbeam, so close to the crystal boundary, extends into the cavity. The atomic ratios, however, suggest continuing increase of iron content towards the rim.

The analyses A4 to A1, with their increasingly lower totals, may serve to illustrate the termination of the scanned crystal against the cavity.

Structural formulae

Annersten (1976) has shown by Mössbauer spectrometry that iron in a natural sanidine (1.3 wt.% Fe_2O_3) is trivalent and occupies the *T*-site. In terrestrial K-feldspars probably most of the iron present is Fe^{3+} replacing Al in the tetrahedral sites (Smith and Brown, 1988). Framework silicates with eight oxygen a.p.f.u. must have four tetrahedrally coordinated cations p.f.u. Reductions of the EMP analyses to such unit formulae

Table 3. Selected SEM analyses[1] and unit formulae[2] of sanidine of Cancarix.

	d.l.	C(core)	A8	A7	C2	A6	C1	A5
SiO_2		64.1	61.7	61.9	63.3	62.5	59.5	55.1
TiO_2	0.20	0.33	n.d	n.d	n.d	n.d	n.d	n.d
Al_2O_3		17.5	9.52	5.84	5.24	4.55	3.99	3.04
$Fe_2O_3^t$		1.24	9.5	13.4	14.0	14.5	14.5	14.2
MgO	0.19	n.d	0.27	0.41	0.24	0.32	0.29	0.47
BaO	0.32	n.d	n.d	n.d	n.d	n.d	n.d	n.d
CaO	0.14	n.d	n.d	0.18	n.d	n.d	n.d	n.d
Na_2O		0.48	0.34	0.43	0.28	0.29	0.31	0.42
K_2O		16.0	15.3	14.6	15.1	15.10	14.3	13.2
Total		99.65	96.65	96.76	98.16	97.26	92.89	86.43
Si		2.98	3.06	3.10	3.13	3.13	3.13	3.12
Ti		0.01	-	-	-	-	-	-
Al		0.96	0.56	0.34	0.31	0.27	0.25	0.20
Fe^3		0.04	0.35	0.50	0.52	0.54	0.57	0.61
Mg		-	0.02	0.03	0.02	0.02	0.02	0.04
Ca		-	-	0.01	-	-	-	-
Na		0.04	0.03	0.04	0.03	0.03	0.03	0.05
K		0.95	0.96	0.93	0.95	0.96	0.96	0.95

1: see Fig.2 for locations; 2: based on eight oxygen; d.l.: detection limit of trace elements; n.d.: none detected; t: total iron as Fe_2O_3.

show that Si + Al do not fill the four *T*-sites (Table 2). Including Fe^{3+} as a *T*-site ion, the values for $\Sigma(Si,Al,Fe^{3+})$ vary from 3.960 to 3.991 a.p.f.u., close to four within the accuracy of the analytical method. However, allotment of also Mg in the *T*-sites results in even smaller deviations: $\Sigma(Si,Al,Fe^{3+},Mg)$ = 3.986–3.999 a.p.f.u. The cation totals closely approximate the ideal 5 a.p.f.u. in five analysed spots, viz. 4.992 to 5.008 a.p.f.u.; the one exception of a low 4.968 a.p.f.u. in spot #6 is a consequence of vacancies in the *M*-site due to substantial solid solution with $\square Si_4O_8$ (see later).

Table 4. Cell dimensions and optical properties of sanidine of Cancarix and from the literature

	1	2	3
a, (Å)	8.602(2)	8.598(15)	8.608
b, (Å)	13.036(4)	13.050(26)	13.065
c, (Å)	7.174(2)	7.209(17)	7.199
ß, (°)	116.03(2)	116.00(18)	116.00
V, (Å^3)	722.9(3)	727.1(20)	727.7
2Vα, (°)	44-58*	37-43	56
orientation O.A.P.	//(010)*	//(010)	//(010)
Fe-or (mole %)	0	3-12	14

1. End-member high sanidine (Ferguson et al., 1991),
* optical data inferred from structural data;
2. sanidine of Cancarix (this paper);
3. sanidine of Moon Canyon (Best et al., 1968).

Because the *M*-site occupancy in the feldspar structure is limited to one a.p.f.u., higher ΣM values ought to be scrutinised. With Mg as an *M*-site atom, ΣM = 1.008–1.043, whereas Mg in the *T*-site leads to ΣM = 0.982–1.019 a.p.f.u. The somewhat better ΣT and ΣM values based on Mg as a *T*-site atom seem to support earlier indications in this direction (Smith and Franks, 1986).

Although the calculated formulae are close to MT_4O_8, there are significant departures from the ideal feldspar formula

$$^{M}[R^{+}_{1-a}R^{2+}_{a}]_{\Sigma 1}{}^{T}[R^{2+}_{b}R^{3+}_{1+a-2b}Si_{3-a+b}]_{\Sigma 4}O_8.$$

With respect to the EMP results, four formulae show Si > 3 a.p.f.u. and five show a surplus of the large cations over the trivalent cations, which cannot be justified by the presence of Mg^{2+} in the *T*-site. The thus observed nonstoichiometry may be analysed as follows. After attributing the available elements to $(Na,K)Mg_{0,5}Si_{3,5}O_8$ (Smith and Franks, 1986), celsian, albite, orthoclase, and Fe-orthoclase molecules, there are remainders which cannot be combined into feldspar formulae (Table 2). The three Fe-rich compositions are significantly nonstoichiometric. They deviate substantially from the ideal feldspar formula by having surplusses of K^+ ions over the large

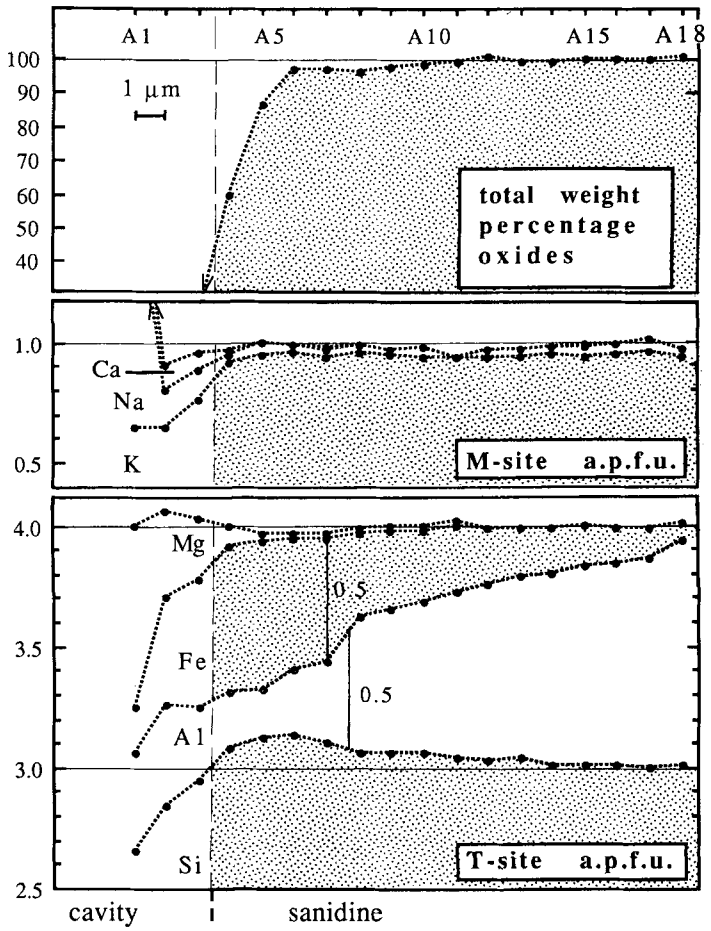

FIG. 3. SEM step scan profile across Fe-rich rim of sanidine. Cumulative diagrams illustrate the fillings of the M- and T-sites. Note that within 3 to 4 μm from the rim the feldspar has over 0.5 Fe^{3+} p.f.u. Low totals at sites A4 and A5 are a consequence of their proximity to the rim of the crystal, see text.

cations needed for feldspar stoichiometry, amounting to 2.7–6.1 at.% and surplusses of 3.8–9.9 at.% Si^{4+}. The unit formula of spot #6 shows a prominent dominance of Fe^{3+}-feldspar (50 mole %) over Al-feldspar (38 mole %).

The SEM analyses, particularly those in the Fe-rich rims, corroborate the nonstoichiometry; again the Si contents are well over 3 a.p.f.u., and the *M*-site cations (excl. those coupled with Mg in the *T*-site) strongly prevail over the trivalent ions in the *T*-site (Table 3). Although the totals of SEM spots A5 and C1 are somewhat low, the resulting formulae are close to MT_4O_8. Also the trends towards the rim for the various elements are continuous to site *A*5 inclusive. So these analyses (A5, C1) demonstrate the existence in sanidine of 57 and 61 mole % of the $[FeSi_3O_8]^{-1}$ component.

Discussion and conclusions

Size and habit of sanidine crystals dependent on cooling conditions and melt composition

For a post-extrusion phase, the sanidine formed rather sizeable crystals. However, in experiments with melts of the composition $(Na_{0.5}K_{0.5})Si_3AlO_8$ containing 2.8 wt.% H_2O, alkali-feldspar crystals grew at rates of 6 mm per day at about 750 °C, implying an undercooling of 200 °C (Fenn, 1977). Obviously, long time periods are not needed to produce coarse feldspar crystals in melts. At small degrees of undercool-

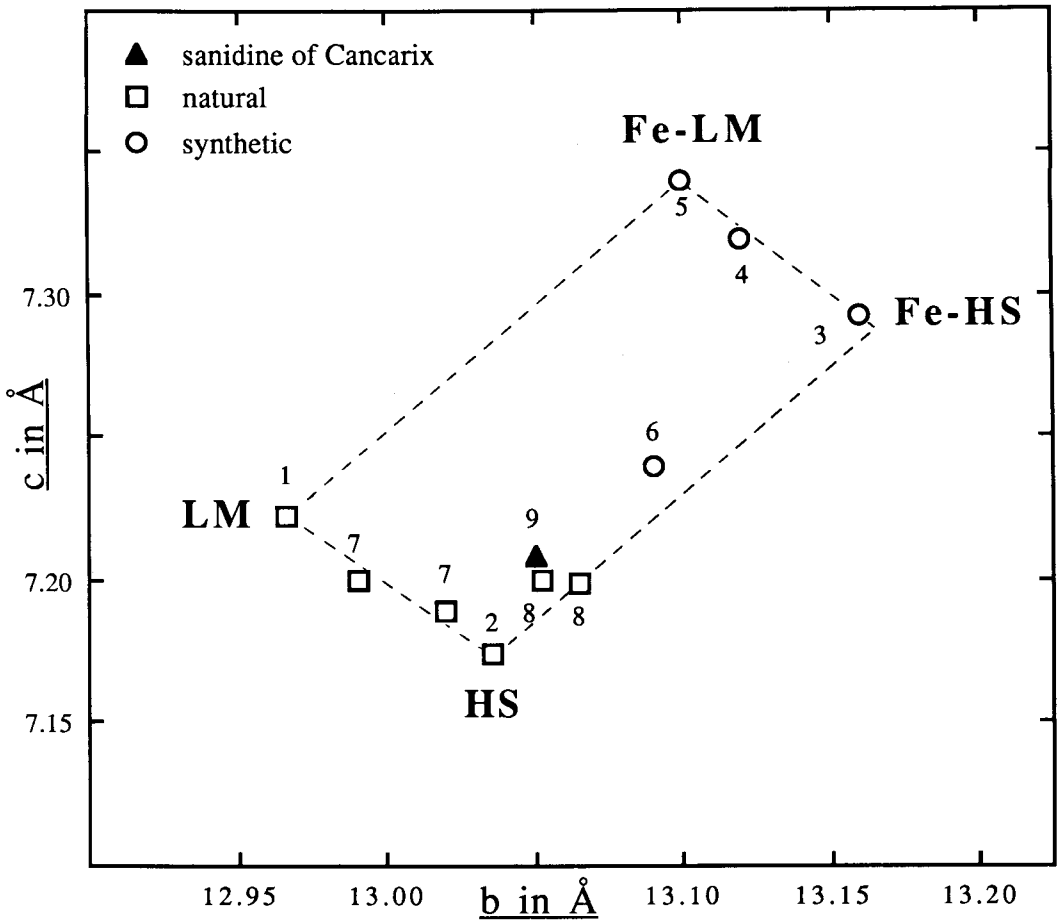

FIG. 4. Plots of *b*–*c* lattice parameters of Fe-bearing and Fe-rich K-feldspars and of (near) end-members of KAl- and KFe-feldspars. LM = low microcline; HS = high sanidine; Fe-LM = low iron-microcline; Fe-HS = high iron-sanidine; 1 Smith and Brown (1988); 2 Ferguson *et al.* (1991); 3 Pentinghaus and Dora (1976); 4 Wones and Appleman (1961); 5 Wones and Appleman (1963); 6 Lindqvist (1966); 7 Coombs (1954); 8 Best *et al.* (1968); 9 This paper.

ing crystals are expected to have smooth planar surfaces, dendritic and spherulitic being the habit of crystals grown under large undercooling (Kirkpatrick, 1975). Since the skeletons of the Cancarix sanidine display an intermediate morphology, a crystallisation under less extreme undercooling is indicated. Considering that the crater was filled by one huge eruption of magma which was immediately isolated by a glassy crust, a moderate undercooling is quite conceivable.

The skeletons also indicate a high crystallisation rate, which is facilitated by supersaturation and high diffusion, the latter strongly dependent on a low viscosity of the melt. Supersaturation of the feldspar component occurred during the extrusion of the magma, due to pressure release and diopside fractionation. Corroborating field evidence, a very low viscosity is apparent from the following. The presence of *ac*, *ns* and *ks* in the CIPW norm shows that the cancalite magma was peralkaline, even perpotassic. The perpotassic character is embodied partly in the subaluminous sanidine itself, but much more strongly in the later crystallising titanian potassium-richterite and dalyite; moreover, the amphibole contains H_2O and F. It will be clear that the formation of sanidine proceeded in an increasingly perpotassic and volatile-rich melt. Peralkalinity, as shown by experiments (Riebling, 1966) and explained by silicate melt theory (e.g. Mysen, 1983), drastically lowers the viscosity of silicate melts and facilitates feldspar crystallisation (Schairer and Bowen,

1955). The presence of H_2O and F will depolymerise the melt structure, thereby contributing to a still lower viscosity (Dingwell and Mysen, 1985). In this context, it is instructive to note that Mustart (1969) has reported the growth of up to 2 mm single crystals from melts fluxed with hydrous alkali-disilicate solutions.

The typically equant to elongate Baveno habit of the Cancarix sanidine, also observed in Fe-bearing sanidines from other lamproite occurrences (Carmichael, 1967; Best *et al.*, 1968), points to a crystallisation temperature of about 1000 K, and not much higher, as that would have caused the growth of the {010}-dominated, platy, Finistere habit (Smith and Brown, 1988).

Equilibration and subsequent quenching

Sanidines rapidly and reversibly change 2V on annealing dependent on temperature and composition (Bertelmann *et al.*, 1985); extrapolating their data, the composition and $2V\alpha$ of the sanidine of Cancarix suggest an equilibration temperature of about 725 °C (Smith and Brown, 1988).

Continued slow cooling from this point would have caused the inversion to low sanidine at about 700 °C (Smith and Brown, 1988) and eventually to a triclinic structure [the iron-sanidine to iron-microcline transition takes place at 704(6) °C; Wones and Appleman (1963)], and possibly also to the exsolution of quartz (and potassium tetrasilicate). None of these phenomena could be observed. So, quenching from about 725 °C is indicated.

A likely cause for quenching is boiling in response to crystallisation from the cooling hydrous peralkaline residual melt. This 'retrograde boiling' (Correns, 1968), at 'the second boiling point' (Krauskopf, 1967), implies vapour pressures exceeding the confining pressure. In the near-surface condition of the volcanite of Cancarix, the pressure inside the cavities conceivably reached values beyond the strength of the rock fabric. The sudden loss of heat, attending the consequent escape of the volatiles from the rock, may well explain the quenching of the disordered structural state of the sanidine.

The escape of the water-rich phase also explains the total absence of late-stage alteration products in the cancalite.

Nonstoichiometry of sanidine

In tectosilicates, nonstoichiometry is by no means rare. It is normal for natural nepheline, in which up to 10 wt.% extra SiO_2 has been found (Tilley, 1954; Hamilton, 1961; Woolley and Platt, 1986). Carmichael (1967) established nonstoichiometry for most leucite from lamproites by demonstrating molecular excess of K_2O and SiO_2. Experiments along the join $CaAl_2Si_2O_8$–SiO_2 have shown that anorthite at the eutectic incorporates 8 wt.% SiO_2 in solid solution (Ito, 1976; Longhi and Hays, 1979). Plagioclase crystals from some lunar basalts have up to 7.5 mole percent $\square Si_4O_8$ (Beaty and Albee, 1980). Carman and Tuttle (1963) found 0.7–2.4 wt.% extra SiO_2 in Na plagioclases and sanidines from granites and rhyolites, and none in sanidines from trachytes and phonolites. These cases have led to the conclusion that nonstoichiometry in tectosilicates is favoured by high temperature, rapid nonequilibrium growth, that the types of the additional phases are related to the composition of the melt, and that the exsolution of the extra components is prevented by rapid cooling. In the Cancarix sanidine, the likelihood that quenching took place at about 725 °C, has been already argued above. The incorporation of extra SiO_2 and K_2O strongly increases across the iron-rich rims of the crystals, which suggests high-rate crystallisation from an increasingly SiO_2- and K_2O-rich residual magma. The rapid growth was facilitated by high diffusion, due to a progressively lower viscosity as a corollary to the concomitant build-up of alkalis and volatiles.

Schairer and Bowen (1955) have shown in experiments in the SiO_2–K_2O–Al_2O_3 system, that K-feldspar may coexist with quartz and K-tetrasilicate in a eutectic at 710 ± 20 °C. Experiments, producing Fe-orthoclase, in the pseudobinary system $K_2O.Si_6O_{12}$–Fe_2O_3 have shown a minimum of the liquidus at 740 °C (Faust, 1936). In the ternary system SiO_2–K_2O–Fe_2O_3 this minimum most probably represents the equivalent of the above-mentioned eutectic. We tentatively suggest that the significant nonstoichiometry, formed during the final stages of growth of the sanidine of Cancarix, represents solid solution of Fe-rich sanidine with K-tetrasilicate and quartz close to their ternary eutectic. If this is so, the nonstoichiometric Fe-rich sanidine was formed at a temperature between 710 ± 20 and 740 °C, which agrees well with the equilibration temperature of about 725 °C, estimated for the bulk of the crystals. Our findings are in good agreement with late-magmatic temperatures ranging down to 740 °C and subsolidus temperatures below 730 °C for lamproites from the same region, as established on the basis of ilmenite–magnetite and phlogopite–apatite geothermometry by Venturelli *et al.* (1988).

Acknowledgements

Electron microprobe facilities were provided by De Vrije Universiteit and by WACOM, a working group for analytical geochemistry subsidised by The Netherlands Organisation for Scientific Research (NWO). We thank Henk Helmers for discussions, Ernst Burke and Piet Maaskant for constructive comments on the manuscript, and Angélina Souren for help with the figures.

References

Annersten, H. (1976) New Mössbauer data on iron in potash feldspar. *Neues Jahrb. Mineral., Mh.*, 337–43.

Beaty, D. W. And Albee, A. L. (1980) Silica solid solution in natural plagioclase. *Am. Mineral.*, **65**, 63–74.

Bertelman, D., Förtsch, E., and Wondratschek, H. (1985) On the annealing behaviour of sanidines: the exceptional case of Eifel sanidine megacrystals. *Neues Jahrb Mineral., Abh.*, **152**, 123–41.

Best, M. G., Henage, L. F., and Adams, J. A. S. (1968) Mica peridotite, wyomingite, and associated potassic igneous rocks in northeastern Utah. *Am. Mineral.*, **55**, 1041–8.

Carman, J. H. and Tuttle, O. F. (1963) Experimental verification of solid solution of excess silica in sanidine from rhyolites. *Program G.S.A. Meeting New Orleans*, 331.

Camichael, I. S. A. (1967) The mineralogy and petrology of the volcanic rocks from the Leucite Hills, Wyoming. *Contrib. Mineral. Petrol.*, **15**, 24–66.

Coombs, D. S. (1954) Ferriferous orthoclase from Madagascar. *Mineral. Mag.*, **30**, 409–27.

Correns, C. W. (1968) *Einführing in die Mineralogie*, 2nd ed. Springer-Verlag, Berlin. 458 pp.

Dingwell, D. B. and Mysen, B. O. (1985) Effects of water and fluorine on the viscosity of albite melt at high pressure: a preliminary investigation. *Earth Planet. Sci. Lett.*, **74**, 266–74.

Faust, G. T. (1936) The fusion relations of iron-orthoclase, with a discussion of the evidence of the existence of an iron-orthoclase molecule in feldspars. *Am. Mineral.*, **21**, 735–63.

Fenn, P. M. (1977) The nucleation and growth of alkali feldspars from hydrous melts. *Can. Mineral.*, **15**, 135–61.

Ferguson, R. B., Ball, N. A., and Černy, P. (1991) Structure refinement of an adularian end-member high sanidine from the Buck Claim pegmatite, Bernic Lake, Manitoba. Ibid., **29**, 543–52.

Fuster, J. M., Gastesi, P., Sagredo, J., and Fermoso, M. L. (1967) Las rocas lamproíticas del S.E. de España. *Estudios Geológicos*, **23**, 35–49.

Hamilton, D. L. (1961) Nephelines as crystallisation temperature indicators. *J. Geol.*, **69**, 321–9.

Hautefeuille, P. and Perrey, A. (1888) Sur la préparation et les propriétés d'orthose ferrique. *Compt. Rend. Acad. Sci. Paris*, **107**, 1150–52.

Ito, J. (1976) High temperature solvent growth of anorthite on the join $CaAl_2Si_2O_8$–SiO_2. *Contrib. Mineral. Petrol.*, **59**, 187–94.

Kirkpatrick, R. J. (1975) Crystal growth from the melt: A review. *Am. Mineral.*, **60**, 798–814.

Krauskopf, K. B. (1967) *Introduction to geochemistry.* McGraw-Hill Book Company, New York, 721 pp.

Kroll, H. and Ribbe, P. H. (1987) Determining (Al,Si) distribution and strain in alkali feldspars using lattice parameters and diffraction-peak positions: a review. *Am. Mineral.*, **72**, 491–506.

Le Maitre, R. W. (1989) *A classification of igneous rocks and glossary of terms: recommendations of the International Union of Geological Sciences Subcommission of the Systematics of Igneous Rocks.* Blackwell Scientific Publications, London. 193 pp.

Lindqvist, B. (1966) Hydrothermal synthesis studies of potash-bearing sequioxide-silica systems. *Geol. Fören. Stockh. Förh.*, **88**, 133–78.

Lindsley, D. H., Smith, D., and Haggerty, S. E. (1971) Petrography and mineral chemistry of a differentiated flow of Picture Gore basalt near Spray, Oregon. *Carnegie Institution Washington Yearbook*, **69**, 264–90.

Linthout, K., Nobel, F., and Lustenhouwer, W. (1988) First occurrence of dalyite in extrusive rock. *Mineral. Mag.*, **368**, 705–8.

Longhi, J. and Hays, J. F. (1979) Phase equilibria and solid solution along the join $CaAl_2Si_2O_8$–SiO_2. *Am. J. Sci.*, **279**, 876–90.

Mitchell, R. H. and Bergman, S. C. (1991) *Petrology of lamproites.* Plenum Press, New York, 447 pp.

Mustart, D. A. (1969) Hydrothermal synthesis of large single crystals of albite and potassium feldspar. *EOS, Trans. Am. Geophys. Union*, **56**, 1075 (Abstr.).

Mysen, B. O. (1983) The structure of silicate melts. *Ann. Reviews Earth Planet. Sci.*, **11**, 75–97.

Nixon, P. H., Thirlwell, M. F., Buckley, F., and Davies, C. J. (1984) Spanish and Western Australian lamproites: aspects of whole rock geochemistry. pp. 285–96. In *Kimberlites and related rocks* (Kornprobst, J., ed.), Elsevier, Amsterdam.

Pentinghaus, H. and Doras, O. Ö. (1976) Strukturelle Zustände in Orhtoklasen von Madagaskar. *Fortschr. Mineral.*, **54**, Bh. 1, 72–3.

Riebling, E. F. (1966) Structure of sodium aluminosilicate melts containing at least 50 mole % SiO_2 at 1500 °C. *J. Chem. Phys.*, **44**, 2857–65.

Schairer, J. F. And Bowen, N. L. (1955) The system K_2O–Al_2O_3–SiO_2. *Am. J. Sci.*, **253**, 681–746.

Smith, J. V. And Brown, W. L. (1988) *Feldspar Minerals, I, Crystal structures, physical, chemical, and microtextural properties*, 2nd ed. Springer Verlag, Berlin, 828 pp.

Smith, P. M. and Franks, P. C. (1986) Mg-rich hollow sanidine in partially melted granite xenoliths in mica peridotite at Rose dome, Woodson County, Kansas. *Am. Mineral.*, **71**, 60–67.

Spencer, E. (1937) The potash-soda feldspars. I. Thermal stability. *Mineral. Mag.*, **24**, 453–94.

Su, S. C., Ribbe, P. H., and Bloss, F. D. (1986) Alkali feldspars: Structural state determined from composition and optic axial angle 2V. *Am. Mineral.*, **71**, 1285–96.

Tilley, C. E. (1954) Nepheline-alkali feldspar paragenesis. *Am. J. Sci.*, **252**, 65–75.

Venturelli, G., Di Battistini, G., Crawford, A. J., Kogarko, L. N., Celestini, S. (1984) The ultrapotassic rocks from southeastern Spain. *Lithos,* **17**, 37–54.

——Salvioli Marani, E., Foley, S. F., Capedri, S., and Crawford, A. J. (1988) Petrogenesis and conditions of crystallisation of Spanish lamproitic rocks. *Can. Mineral.*, **26**, 67–79.

Wagner, C. and Velde, D. (1986) The mineralogy of K-richterite-bearing lamproites. *Am. Mineral.*, **71**, 17–37.

Woensdregt van, C. F. (1982) Crystal morphology of monoclinic potassium feldspars. *Zeits. Krist.*, **161**, 15–33.

Wones, D. R. and Appleman, D. E. (1961) X-ray crystallography and optical properties of synthetic monoclinic $KFeSi_3O_8$, iron-sandine. *U.S.G.S. Prof. Paper,* **424-C**, 309–10.

——(1963) Properties of synthetic triclinic $KFeSi_3O_8$, iron-microcline, with some observations on the iron-microcline $\rightleftharpoons$ iron-sanidine transition. *J. Petrol.*, **4**, 131–7.

Woolley, A. R. and Platt, R. G. (1986) The mineralogy of nepheline syenite complexes from the northern part of the Chilwa Province, Malawi. *Mineral. Mag.*, **50**, 597–611.

[*Manuscript received 3 April 1992: revised 22 May 1992*]